UCRL--102758

DE90 011204

APPLICATIONS OF STRAINED LAYER SUPERLATTICES

D. L. Smith and B. K. Laurich
Los Alamos National Laboratory

C. Mailhiot
Lawrence Livermore National Laboratory

This paper was prepared for the proceedings of the
MRS Spring Meeting: Atomic Scale Calculations of Structure in Materials
San Francisco, CA April 16 - 21, 1990

April 1990

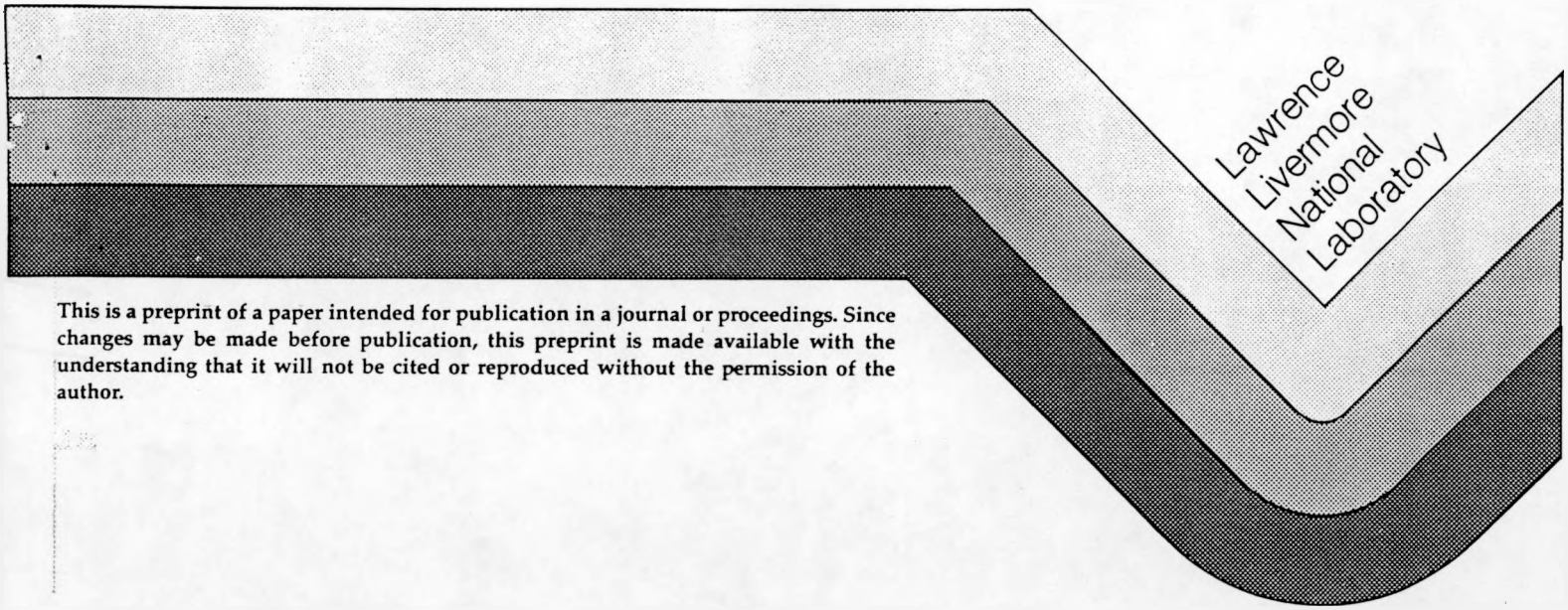

APPLICATIONS OF STRAINED LAYER SUPERLATTICES

D. L. SMITH*, B. K. LAURICH* AND C. MAILHIOT**
*LOS ALAMOS NATIONAL LABORATORY, Los Alamos, NM 87545
**LAWRENCE LIVERMORE NATIONAL LABORATORY, Livermore, CA 94550

ABSTRACT

Because of different band-edge lineups, strain conditions, and growth orientations, various strained-layer superlattice (SLS) materials can exhibit qualitatively new physical behavior in their optical properties. We describe two examples of new physical behavior in SLS: strain-generated electric fields in polar growth axis superlattices and strained type II superlattices. In SLS, large electric fields can be generated by the piezoelectric effect. The fields are largest for SLS with a [111] growth axis; they vanish for SLS with a [100] growth axis. The strain generated electric fields strongly modify the optical properties of the superlattice. Photogenerated electron-hole pairs screen the fields leading to a large nonlinear optical response. Application of an external electric field leads to a large linear electrooptical response. The absorption edge can be either red or blue shifted. Optical studies of [100], [111], and [211] oriented GaInAs/GaAs superlattices confirm the existence of the strain-generated electric fields. Small band gap semiconductors are useful for making intrinsic long wavelength infrared detectors. arbitrarily small band gaps can be reached in the type II superlattice InAs/GaSb. However, for band gaps less than 0.1 eV, the layer thicknesses are large and the overlap of electron and hole wavefunctions are small. Thus, the absorption coefficient is too small for useful infrared (IR) detection. Including In in the GaSb introduces strain in he InAs/GaInSb superlattice which shifts the band edges so that small band gaps can be reached in thin layer superlattices. Good absorption at long IR wavelengths is thus achieved.

INTRODUCTION

Pseudomorphic growth of thin semiconductor layers, whose lattice constant differs from that of the substrate upon which it is grown, has been clearly demonstrated [1-3]. For material layers thinner than a critical thickness, which depends on the difference in lattice constants, the lattice mismatch is accommodated by internal strain in the film rather than by the formation of dislocations. The internal strain can produce novel physical properties in SLS [4]. Here we consider two examples of strain induced

properties: electric fields generated by the piezoelectric effect and strained type II superlattices. Large electric fields occur in SLS grown along a polar axis such as [111] or [211] (see Ref. 5). These fields strongly modify the optical properties of the SLS [6]. The fields can be modulated by screening from photogenerated electron-hole pairs [7] and by application of an external field [8] leading to nonlinear optical and electrooptical response, respectively. Strain can be used to tailor the optical response of type II superlattices for long wavelength IR detector applications. In particular, the strained type II superlattice In/As/GaInSb shows promise for this application [9,10].

Strain Generated Electric Fields

The III-V semiconductors are piezoelectric. Therefore, strains in the material can generate polarization fields. To generate a polarization field, it is necessary that the strain have off-diagonal components in a zincblend structure material. To put this another way, the 90° angles in the cubic unit cell must be distorted by the strain if a polarization field is to be generated. In a [100] SLS, the strains are along the faces of the cubic unit cell. The fours side faces are distorted from squares to rectangles, but the angles all remain 90°, and the polarization fields directed along the growth axis are generated. In a [110] SLS, polarization fields directed in the superlattice plane are generated. In general, the polarization fields have components along both the growth axis and in the superlattice plane.

The polarity of the polarization field changes abruptly at the superlattice interfaces because the signs of the lattice-mismatch-induced strains are opposite in the two constituent materials making up the SLS. A sign change in a component of polarization along the growth axis gives a sheet of divergence of polarization, that is a sheet of polarization charge. This polarization charge generates electric fields which point along the growth axis. A sign change in a component of polarization in the superlattice plane gives a sheet of curl of polarization. This does not correspond to a polarization charge and does not generate an electric field. For example, in a [110] SLS, the polarization field lies entirely in the superlattice plane and does not generate electric fields. In general, the strain-generated electric fields lie entirely along the growth axis and do not have components in the superlattice plane [11]. In Fig. 1, we show a calculation of the magnitude of the strain-generated electric field in a GaInAs/GaAs ISES with 20% In and equally thick GaAs and GaInAs layers as a function of growth direction. The orientation of the growth axis is expressed in spherical coordinates. The azimuthal angle is fixed at 45° and the polar angle is scanned. For a [100] growth axis, no polarization fields and thus no electric fields are generated. For a [110] growth axis, the polarization field lies in the superlattice plane and does not generate an electric field. For

other growth directions electric fields oriented along the superlattice growth axis are generated. The maximum size of the electric field occurs for a [111] growth axis. For this case, the polarization fields are along the growth axis. For other growth directions, there is also a component of polarization in the superlattice plane which does not contribute to generating the electric field. The size of the strain generated electric fields can exceed 10^5V/cm for a modest lattice mismatch of 1.4%.

Nonlinear Optical Properties

The strain-generated electric fields significantly change the electronic structure and hence the optical properties of the ISES. They shift the fundamental absorption edge to lower energy and change optical selection rules [6]. In a conventional [100] superlattice, there is a strong optical transition between the first heavy-hole subband (hh_1) and the first conduction subband (C_1), whereas the hh_2-C_1 transition is forbidden by an inversion selection rule. In ISES, the inversion symmetry is lost and the hh_2-C_1 transition becomes strong. In Fig. 2, we show calculations of the resonant contribution to the index of refraction (a frequency independent constant is added to the resonance contribution to get the total index of refraction) and the absorption coefficient near the fundamental absorption edge for a [111] ISES consisting of 25 molecular layers (84Å) of $GA_{0.47}In_{0.53}As$ alternating with 50 molecular layers (167Å) of $A1_{0.7}In_{0.3}As$. The lattice mismatch is 1.5%. The strain-induced electric field is $1.4 \cdot 10^5$V/cm in the Ga alloy and half this value in the A1 alloy. Surface charge accumulation will eliminate any potential drop across the entire superlattice. Thus, the potential drop across each superlatticed period will be zero. In the figure, results are shown for the calculated values of the strain-generated electric fields, E_0. For comparison, a case in which the electric fields are scaled to half their calculated values and a case in which there are no electric fields are also shown. Without the electric field, there is a single strong hh_1-C_1 exciton transition at about 0.90 eV and a very weak hh_3-C_1 transition at about 0.93 eV. As the size of the field is increased toward the calculated value, the hh_1-C_1 exciton transitions shifts to lower energy (0.87 eV) and oscillator strength is transferred to the hh_2-C_1 transition (0.93 eV) and the hh_3-C_1 transition (0.93 eV). Light-hold transitions are at higher energy than shown in the figure because the light-hole band is split off from the heavy-hole band by strain.

If light is absorbed by the ISES, the electric-hole pairs which are generated screen the strain-generated electric fields. Because the electric

fields strongly modify the ISES optical response (Fig. 2), the screening effect leads to a strong optical nonlinearity [7]. In Fig. 3 we show calculated values of the real (top) and imaginary (bottom) parts of the nonlinear susceptibility χ^3 (all frequencies the same) as a function of frequency for an ISES consisting of 20(25) molecular layers of $GA_{0.47}In_{0.53}As$ alternating with 40(50) molecular layers of $A1_{0.7}In_{0.3}As$ in the left (right) panel. Very large values of χ^3 are reached near frequencies corresponding to the exciton resonances.

Electrooptical Properties

By incorporating an ISES in the intrinsic the region of a PIN diode or in a Schottky diode, an external electric field can be directly applied to the ISES. In the ISES, the strain generated electric fields in the quantum wells and in the barriers are of opposite polarity. For superlattices in which the quantum wells are essentially isolated from each other by the barriers, the electric field in the quantum wells is much more important than that in the barriers in determining the superlattice optical response. The externally applied field can either enhance or decrease the strain-generated electric field in the quantum wells. If, as will typically be the case, the applied field is small compared to the strain-generated field in the quantum well, a first-order electrooptical response occurs [8]. If the applied field enhances the strain-generated field in the quantum well, the hh_1-C-$_1$transition is red shifted; whereas, if the applied field decreases the strain-generated field is the quantum well, the hh_1-C-$_1$ transition is blue shifted. In a conventional [100] superlattice, in which there are no strain-generated electric fields, the hh_1-C_1 transition is red shifted for either bias polarity [9]. In Fig. 4, we show calculated values of the linear electrooptical coefficient, r, as a function of frequency for ISES consisting of 25 molecular layers of $Ga_{0.47}In_{0.53}As$ alternating with 50 molecular layers of $A_{10.7}In_{0.3}As$. We also show calculations of two figures of merit for an electrooptical material $\Delta n/\alpha$ (the change in refractive index divided by the zero field absorption coefficient) and $\Delta\alpha/\alpha$ (the change in absorption coefficient divided by the zero field absorption coefficient) as a function of frequency. The linear electrooptical coefficient takes on very large values. For comparison, in KDP, the coefficient r is about 10^{-9}cm/V. The figures of merit have favorable values.

Experimental Results

As shown in Fig. 2, the strain-generated electric fields change the superlattice optical properties qualitatively. In order to verify this behavior

experimental, the optical properties of [100] and [111] SLS were compared. The strain-generated electric fields are the principal difference expected between [100] and [111] superlattices [6]. Only small quantitative changes in the electronic structure and optical properties are expected due to anistropies in effective masses, deformation potentials, etc. Recent experimental work on the lattice-matched GaA1As/GaAs system, where strain-generated [12] electric fields do not occur, has borne out these expectations [12].

Two GaInAs/GaAs SLS samples grown simultaneously by molecular-beam epitaxy on semi-insulating Ga/As substrates were investigated. One sample was grown on a [100] substrate and the other on a [111]B substrate. Each superlattice consisted of twenty periods of 70Å of the GaInAs well and 140Å of the GaAs barrier. Secondary-ion mass spectroscopy profiling was used for layer thickness characterization. Rutherford backscattering indicated that the In composition was 0.10±0.02 atomic percent. The samples were not intentionally doped; but there was carbon incorporating at about the $10^{15}cm^{-3}$ level. Further details of the sample growth and characterization are given elsewhere [13,14,15].

In Fig. 5, we show calculated energy band diagrams for the [100] and [111] SLS. The calculated energy positions of the lowest electron and hole states, relative to the band edges, are also shown. For states with significant dispersion along the growth axis, the bandwidth for k in this direction is indicated. The dominant near gap optical transitions are indicated. The two energy band diagrams are qualitatively different because of the strain-generated electric fields, which are represented by the slanting band edges, in the [111] superlattice. Details of the calculations presented in Fig. 5 are discussed elsewhere [14].

Photoluminescence spectra for the [100] and [111] SLS taken at 4.2 K are shown in Fig. 6. Calculated energy positions from Fig. 5 and the transition assignments are indicated by arrows. The luminescence peak labeled Ic in the [100] SLS is believed to be an electron to bound-acceptor transition. Analogous impurity transitions are seen in the [111] SLS luminescence under different excitation and temperature conditions. The data shown in Fig. 6 is representative of a large set of luminescence data taken at different temperature and excitation conditions and absorption data taken at different temperature conditions [14,15,16]. Comparison among this data set was used in making the transition assignments. The [100] SLS data is well described by the usual model. The [111] SLS data is qualitatively different than the [100] SLS data and cannot be even qualitatively described by a model which neglects the strain-generated fields. However, the [111] SLS data is quantitatively described by the model including the strain-generated electric

fields. These results give strong evidence for the presence of strain-generated electric fields in [111] SLS having the magnitude predicted by elastic theory.

Strained Type II Superlattices

Major efforts have recently been devoted to the fabrication of two-dimensional arrays of photovoltiac detectors for the purpose of IR imaging. The HgCdTe alloy is the material used to fabricate such detector arrays. Large tunneling currents and the requirement of extremely precise composition control to accurately determine the band gap are two major difficulties in making such detector arrays. These problems are especially sever for long wavelength ($\lambda \geq 10\mu m$) applications. Small band gap superlattices have intrinsic advantages compared to the HgCdTe alloy for long wavelength photovoltaic detectors [17]. Here we show that strain can be used to tailor the optical response of type II superlattices for long wavelength IR detector applications.

The InAs/GaSb superlattice is type II in which the conduction band minimum of InAs is lower in energy than the valence band maximum of GaSb. Because of this unusual band alignment, the superlattice can have a band gap smaller than that of either constituent material. In fact, the superlattice can even be metallic. However, because of the band lineup, electrons and holes tend to be localized in adjacent layers: electrons in the InAs and holes in the GaSb. The wavefunction overlap, and consequently the optical matrix element, between electrons and holes decreases rapidly with increasing superlattice layer thickn ess. As a result, the optical absorption coefficient of InAs/GaSb superlattices is too small for IR detector applications in the thick-layer regime where the superlattice band gap corresponds to long IR wavelengths [18]. By alloying the GaSb with InSb, so that the superlattice is InAs/GaInSb, small band gap superlattices can be achieved for sufficiently thin material layers that the spatial separation of electrons and holes is weak. Thus, this superlattice has good optical absorption properties. Alloying the GaSb with InSb increases the lattice constant of the material and causes the superlattice to be strained. Strain effects lead to the favorable optical properties of this superlattice (the lattice constants of InAs and GaSb are nearly equal, 0.6% mismatch, and strain effects in this superlattice are small.)

In Fig. (7a) we show the energy-band positions for unstrained InAs, GaSb and InSb. The conduction band of InAs is 0.1 eV below the valence band of GaSb. This energy band lineup has been measured directly [19]. On the basis of photoemission threshold data [20] and Schottky barrier positions referenced to Au [21], the valance bands of unstrained GaSb and InSb are taken to line up. The effect of strain on the bands are shown in Fig. (7b) for a free standing InAs/$Ga_{0.6}$ $In_{0.4}Sb$ superlattice. The internal strain lowers the

conduction band minimum of InAs and raises the heavy-hole band of GaIn Sb by deformation potential effects. The energy band positions shown in Fig. (7b) are in good agreement with recent calculations by Van de Wall [22]. The superlattice band gap derives from electron states split up from the InAs conduction band minimum and heavy-hole states split down from the GaInSb valence band by quantum confinement effects. Since strain lowers the InAs conduction band minimum and raises the GaInSb valence band maximum, it reduces the superlattice band gap at a given layer thickness. Because small band gap superlattices can be achieved for thin layer InAs/GaInSb SLS, reasonably large optical matrix elements can be obtained and this material system exhibits desirable optical properties at long IR wavelengths.

In Fig. (8) we show the band structure for a superlattice consisting of 11 molecular layers (~32 Å) of InAs and 11 molecular layers of $Ga_{0.6}In_{0.4}Sb$ grown along the [001] direction. Subband dispersion is shown for wavevectors parallel and perpendicular to the growth axis. The band gap of this superlattice corresponds to a cutoff wavelength of 11.2μm. An advantageous feature of the energy-band structure is the large energy dispersion of the electron subband along the growth direct. This large energy dispersion occurs because the superlattice layers are thin so that the electrons are not strongly confined. It leads to good electron transport along the growth axis. The electron effective mass is roughly spherical with a value of 0.05 Mo. This is a convenient value for device design: it is small enough to give good mobilities and diffusivities but large enough to give small diode tunneling currents.

In Fig. (9) we compare the calculated optical absorption coefficient of the superlattice whose band structure is shown in Fig. (8) with a HgCdTe alloy whose composition was chosen to give the same band gap as the superlattice. The absorption coefficients are quite similar in the two materials the optical transition matrix element is larger in the HgCdTe alloy than in the superlattice, but the electron effective mass is smaller in the HgCdTe alloy than in the superlattice. Therefore, the density of final state in the optical transition is smaller in the alloy. These two effects nearly cancel. The HgCdTe alloy and the superlattice have similar absorption properties but the superlattice is expected to have superior electrical properties.

SUMMARY

Strain can introduce interesting new physical properties which are potentially useful in SLS. We have discussed two examples of such properties.

**Work performed under the auspices of the U.S. Department of Energy by the Lawrence Livermore National Laboratory under contract number W-7405-ENG-48.

REFERENCES

1. J. W. Matthews and A. E. Blakeslee, J. Cryst. Growth 27, 118 (1974); 29, 273 (1975); 32, 265 (1976).

2. G. C. Osbourn, R. M. Biefeld, and P. L. Gourley, Appl. Phys. Lett. 42, 172 (1982).

3. I. J. Fritz, L. R. Dawson, and T. E. Zipperian, Appl. Phys. Lett. 43, 846 (1983).

4. G. C. Osbourn, J. Appl. Phys. 53, 1586 (1982).

5. D. L. Smith, Solid State Commun. 57, 919 (1986).

6. C. Mailhiot and D. L. Smith, Phys. Rev. B35, 1242 (1987).

7. D. L. Smith and C. Mailhiot, Phys. Rev. Lett. 58, 1264 (1987).

8. C. Mailhiot and D. L. Smith, Phys. Rev. B37, 10415 (1988).

9. D. L. Smith and C. Mailhot, J. Appl. Phys. 62, 2545 (1987).

10. C. Mailhiot and D. L. Smith, J. Vac. Sci. Technol. A7, 445(1989).

11. D. L. Smith and C. Mailhiot, J. Appl. Phys. 63, 2717 (1988).

12. T. Hayakawa, K. Takahashi, M. Kondo, T. Suyoma, S. Yamamoto, and T. Hijikata, ,Phys. Rev. Lett. 60, 349 (1988).

13. K. Elcess, J. L. Lievin, and C. G. Fonstad, J. Vac. Sci. Technol. B6, 638 (1988).

14. B. K. Laurich, K. Elcess, C. G. Fonstad, J. G. Beery, C. Mailhiot, and D. L. Smith, Phys. Rev. Lett. 62, 649 (1989).

15. J. G. Beery, B. K. Laurich, C. J. Maggiore, D. L. Smith, K. Elcess, C. G. Fonstad, and C. Mailhiot, Appl. Phys. Lett. 54, 233 (1989).

16. B. K. Laurich, D. L. Smith, K. Elcess, C. G. Fonstad, and C. Mailhiot, Superlatt. and Microstruc. 5, 341 (1989).

17. D. L. Smith, T. C. McGill, and J. N. Schulman, Appl. Phys. Lett. 43, 180 (1983).

18. D. K. Arch, G. Wicks, T. Tonaue, and J. L. Staudenmann, J. Appl. Phys. 58, 3933 (1985).

19. G. A. Sai-Halasz, L. L. Chang, J. M. Walter, C. A. Chang, and L. Esaki, Solid State Commun. 27, 935 (1978).

20. G. W. Gobeli and F. G. Allen, Phys. Rev. 137, A245 (1965).

21. C. A. Mead, Solid State Electron. 9, 1023 (1966).

22. C. G. Van de Walle, Phys. Rev. B39, 1871 (1989).

FIGURE CAPTIONS

Fig. 1. Strain-generated electric field in a GaInAs/GaAs SLS as a function of growth direction.

Fig. 2. Resonant contribution to the index of refraction (left) and absorption coefficient (right) as a function of photon energy for three values of the strain-generated fields.

Fig. 3. Real part (top) and imaginary part (bottom) of ψ^3 as functions of photon energy for equal pump and probe frequencies for two superlattice thicknesses.

Fig. 4. Electrooptical coefficients as a function of photon energy.

Fig. 5. Calculated energy band diagrams and electronic state energies for the [100] and [111] oriented SLS.

Fig. 6. Luminescence spectra for [100] and [111] oriented SLS. The theoretically calculated transitions are marked by arrows. Ic indicates impurity-related emission.

Fig. 7. (a) Relative energy positions for unstrained InAs,GaSb and InSb. (b) Effect of internal strain on the energy bands for an InAs/$Ga_{0.6}In_{0.4}Sb$ superlattice.

Fig. 8. Superlattice energy band structure for a free-standing SLS consisting of 11 layers of InAs alternating with 11 layers of $Ga_{0.6}In_{0.4}Sb$ grown along the [001] axis.

Fig. 9. Optical absorption coefficient as a function of photon energy for the superlattice show band structure is shown in Fig. 8, and for a HgCdTe alloy with the same band gap.

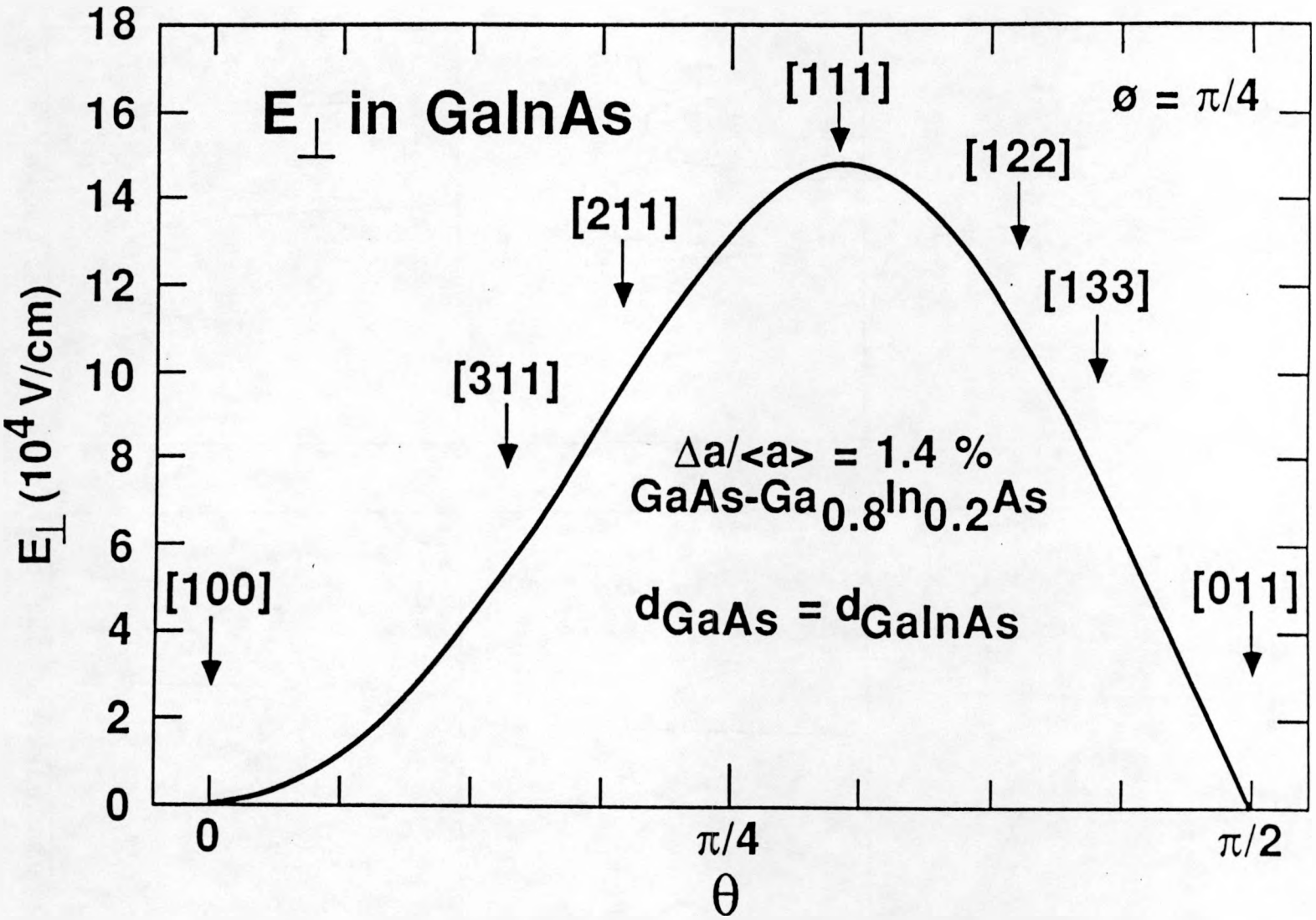
E⊥ in GaInAs
ø = π/4
[111]
[122]
[211]
[133]
[311]
[100]
[011]
Δa/<a> = 1.4 %
GaAs-Ga0.8In0.2As
dGaAs = dGaInAs
E⊥ (10^4 V/cm)
θ
0
π/4
π/2
0
2
4
6
8
10
12
14
16
18

Fig 1.

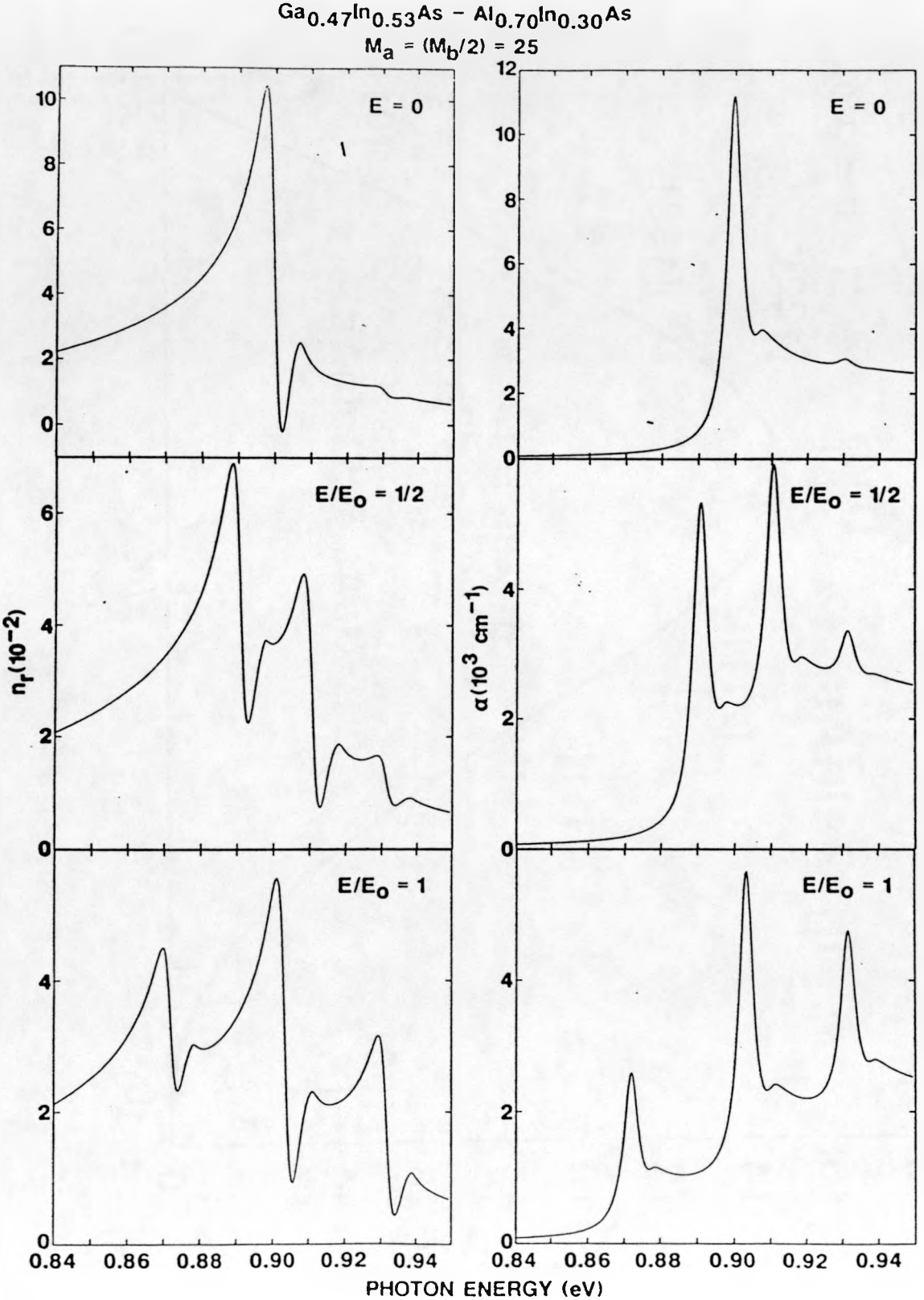
$Ga_{0.47}In_{0.53}As - Al_{0.70}In_{0.30}As$
$M_a = (M_b/2) = 25$
E = 0
E/E$_o$ = 1/2
E/E$_o$ = 1
$n_r(10^{-2})$
$\alpha(10^3\ cm^{-1})$
PHOTON ENERGY (eV)

Fig 2

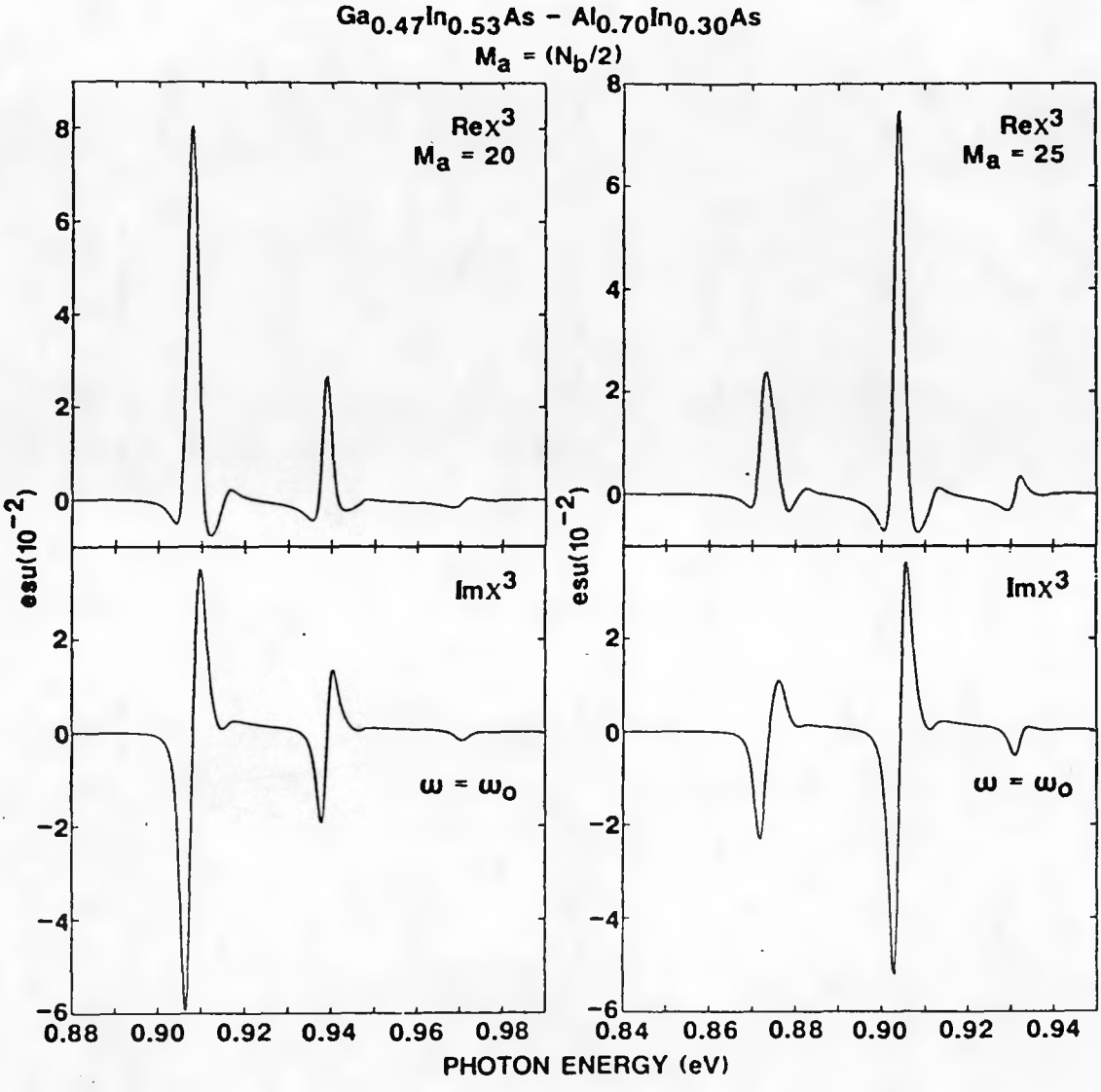
$Ga_{0.47}In_{0.53}As - Al_{0.70}In_{0.30}As$
$M_a = (N_b/2)$
$Re\chi^3$
$M_a = 20$
$Im\chi^3$
$\omega = \omega_o$
$Re\chi^3$
$M_a = 25$
$Im\chi^3$
$\omega = \omega_o$
esu(10^{-2})
esu(10^{-2})
PHOTON ENERGY (eV)

Fig 3

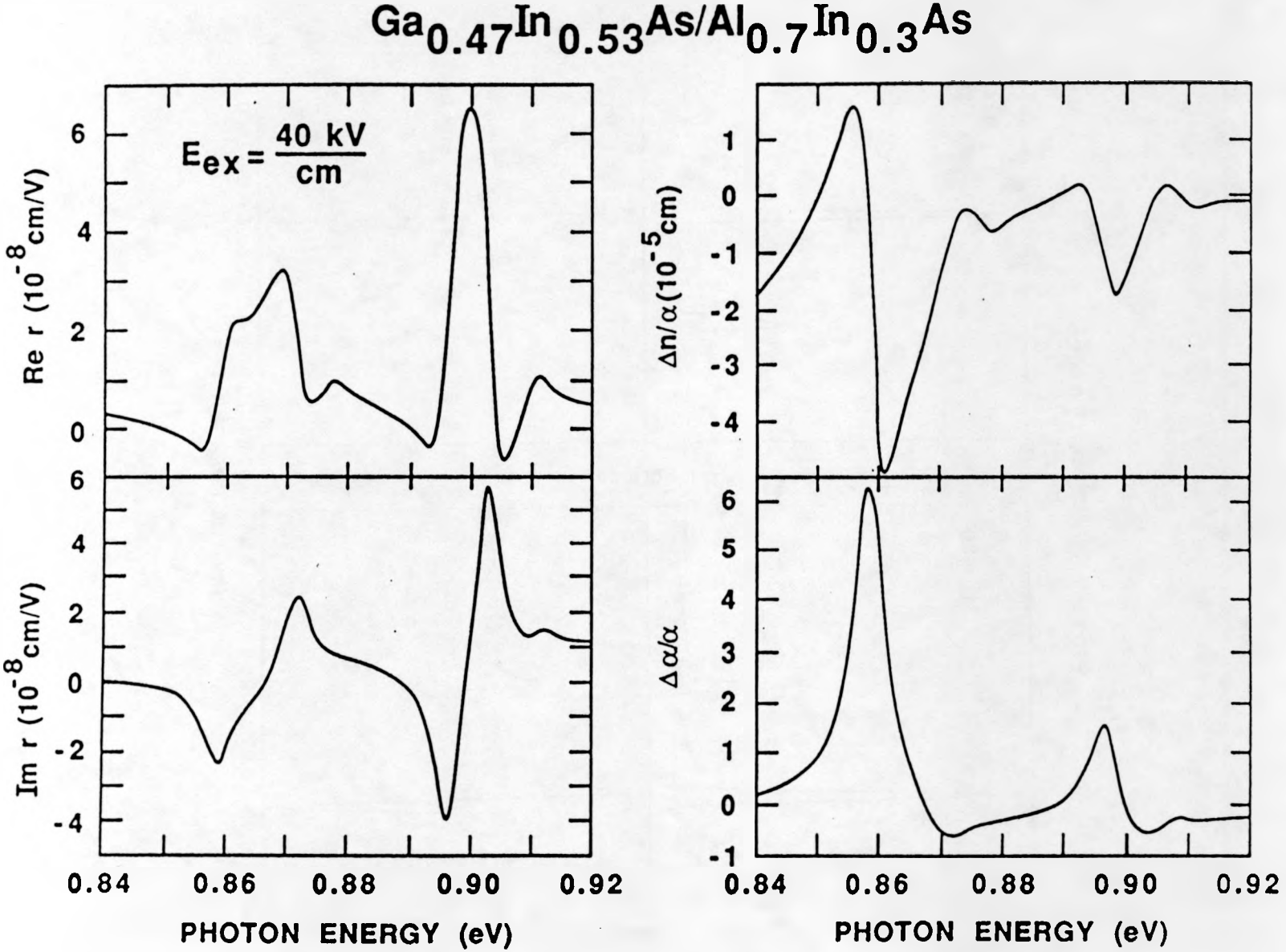
$Ga_{0.47}In_{0.53}As/Al_{0.7}In_{0.3}As$
$E_{ex} = \frac{40\ kV}{cm}$
Re r (10^{-8}cm/V)
Im r (10^{-8}cm/V)
$\Delta n/\alpha$(10^{-5}cm)
$\Delta\alpha/\alpha$
PHOTON ENERGY (eV)
PHOTON ENERGY (eV)

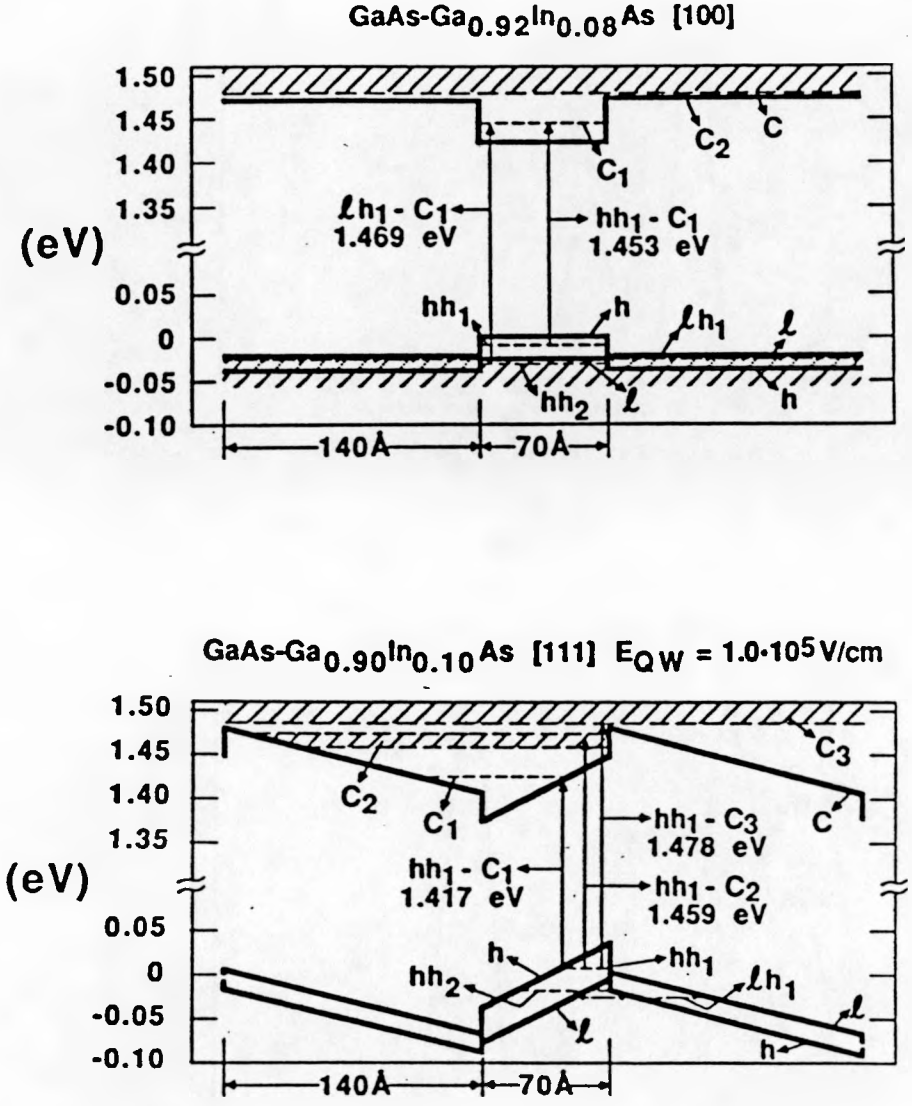
GaAs-Ga0.92In0.08As [100]
1.50
1.45
1.40
1.35
(eV)
0.05
0
-0.05
-0.10
C2
C
C1
lh1 - C1
1.469 eV
hh1 - C1
1.453 eV
hh1
h
lh1
l
hh2
l
h
140Å
70Å
GaAs-Ga0.90In0.10As [111] EQW = 1.0·10^5 V/cm
1.50
1.45
1.40
1.35
(eV)
0.05
0
-0.05
-0.10
C3
C2
C1
C
hh1 - C3
1.478 eV
hh1 - C1
1.417 eV
hh1 - C2
1.459 eV
h
hh1
hh2
lh1
l
l
h
140Å
70Å

Fig 5

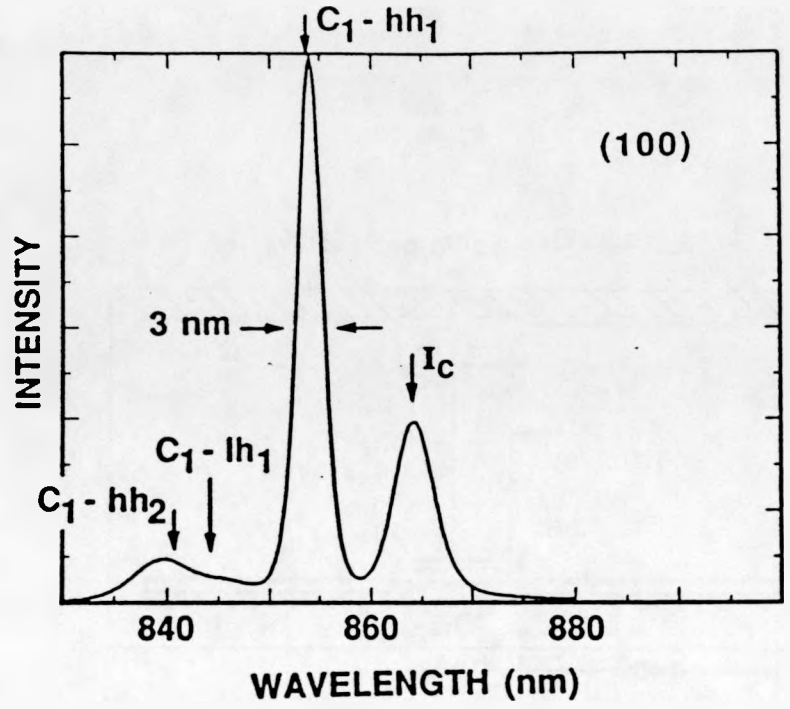
C1 - hh1
(100)
INTENSITY
3 nm
Ic
C1 - lh1
C1 - hh2
840
860
880
WAVELENGTH (nm)

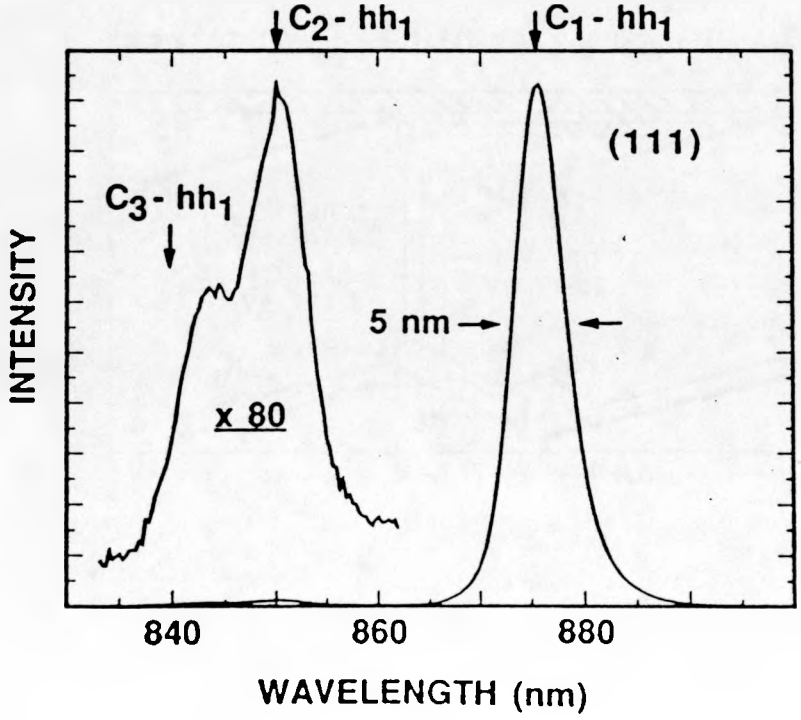
C2 - hh1
C1 - hh1
(111)
C3 - hh1
INTENSITY
5 nm
x 80
840
860
880
WAVELENGTH (nm)

Fig 6

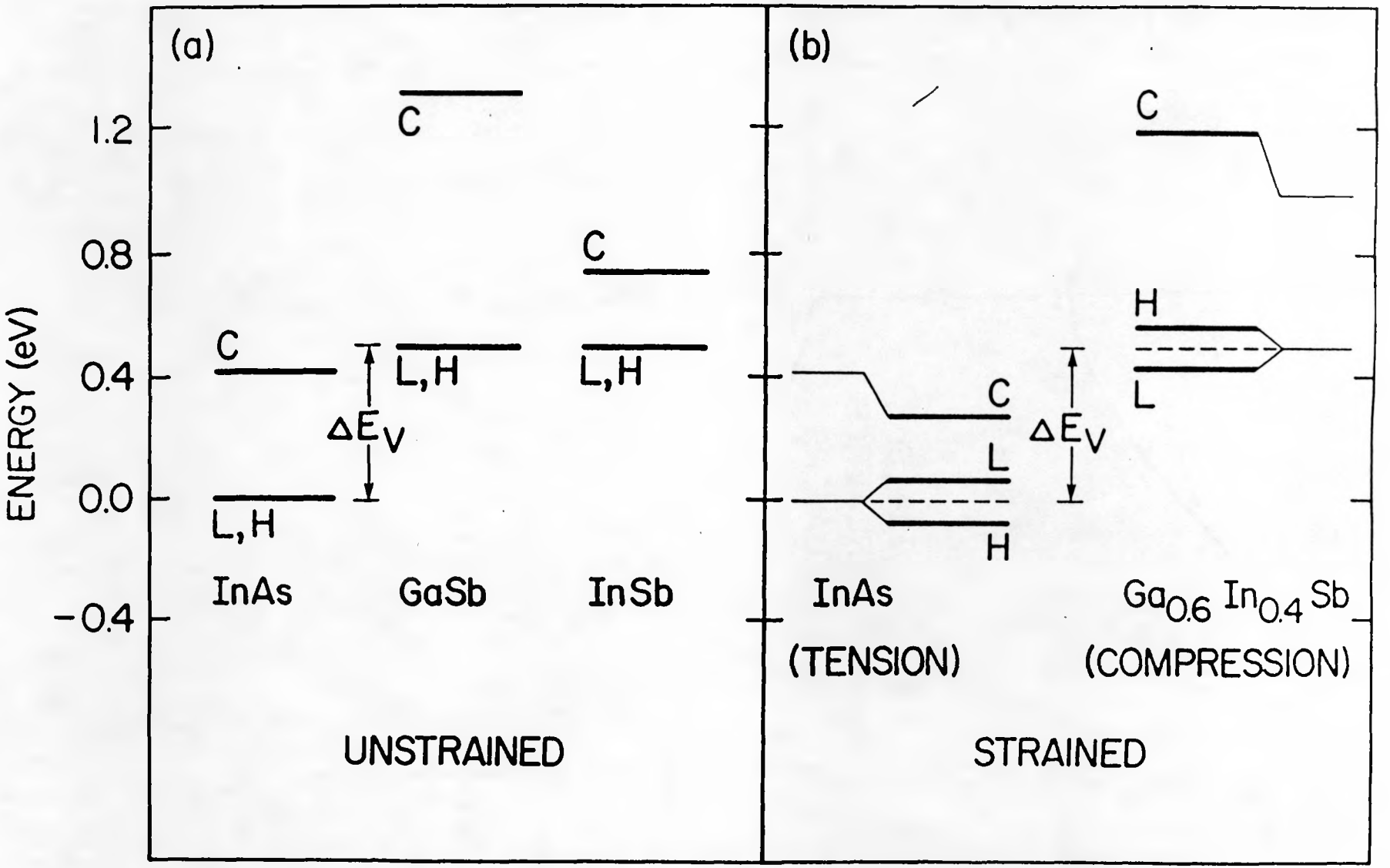
(a)
(b)
ENERGY (eV)
1.2
0.8
0.4
0.0
-0.4
C
C
C
L,H
L,H
L,H
ΔEV
InAs
GaSb
InSb
UNSTRAINED
C
H
L
C
L
H
ΔEV
InAs
(TENSION)
Ga0.6 In0.4 Sb
(COMPRESSION)
STRAINED

Fig 7

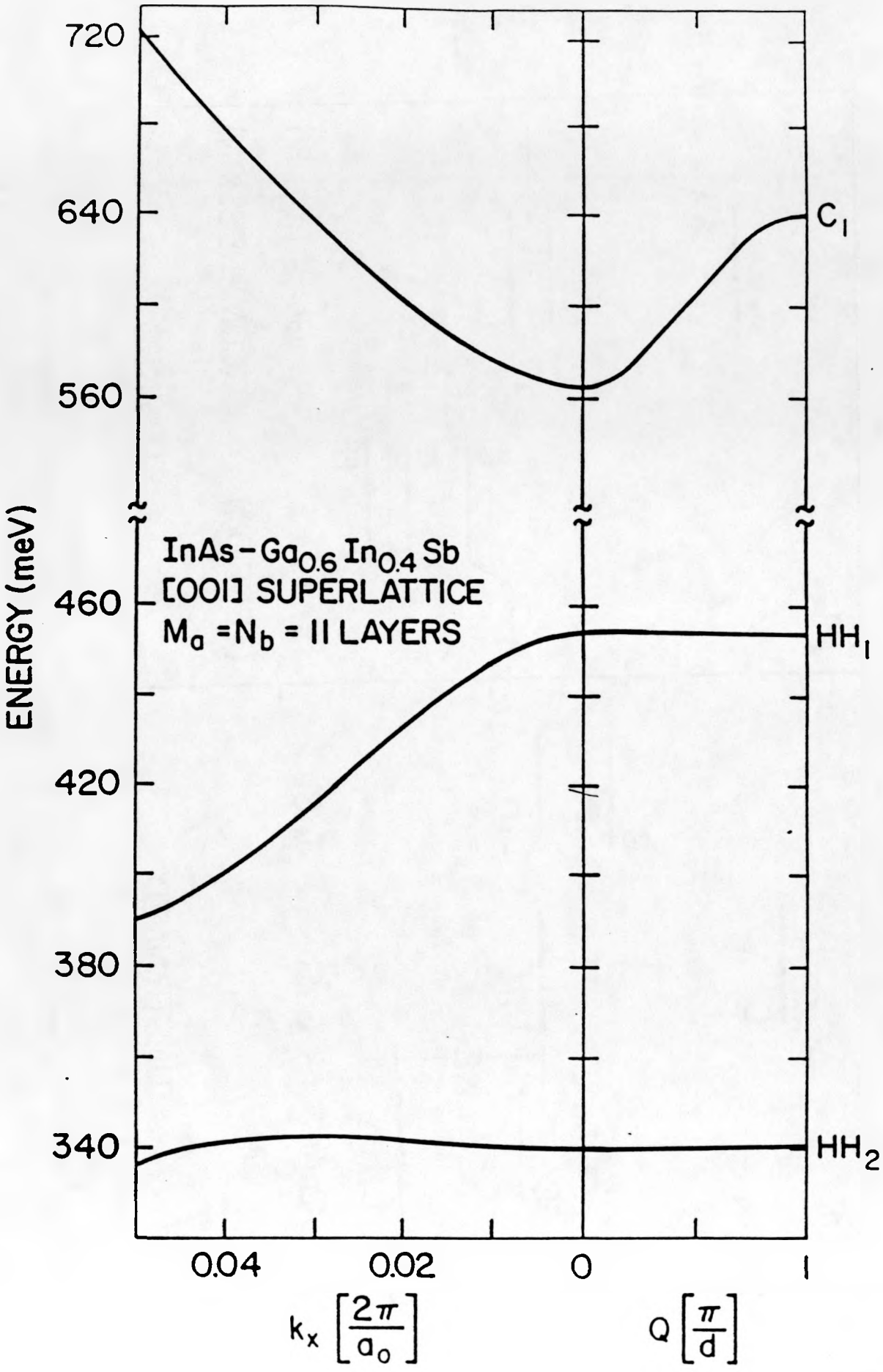
720
640
560
460
420
380
340
ENERGY (meV)
InAs – Ga0.6 In0.4 Sb
[001] SUPERLATTICE
Ma = Nb = 11 LAYERS
C1
HH1
HH2
0.04
0.02
0
1
kx [2π/a0]
Q [π/d]

Fig 8

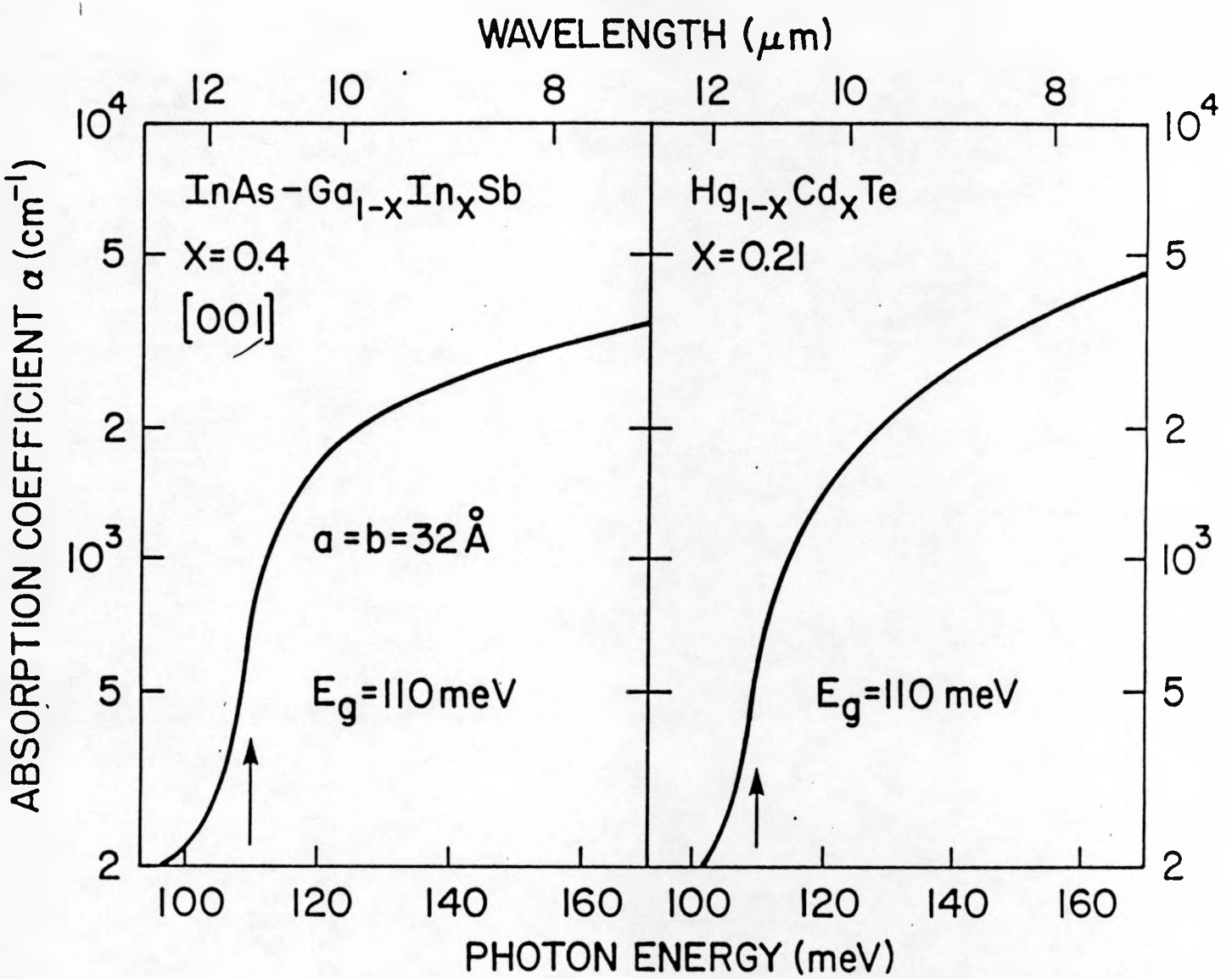
WAVELENGTH (μm)
12
10
8
12
10
8
ABSORPTION COEFFICIENT α (cm⁻¹)
10⁴
5
2
10³
5
2
InAs – Ga1-xInxSb
X=0.4
[001]
a=b=32 Å
Eg=110 meV
Hg1-xCdxTe
X=0.21
Eg=110 meV
100
120
140
160
100
120
140
160
PHOTON ENERGY (meV)

Fig 9